

History-dependent percolation in two dimensions

Minghui Hu,¹ Yanan Sun,¹ Dali Wang,¹ Jian-Ping Lv,^{1,*} and Youjin Deng²

¹*Department of Physics, Anhui Normal University, Wuhu, Anhui 241000, China*

²*National Laboratory for Physical Sciences at Microscale and Department of Modern Physics, University of Science and Technology of China, Hefei, Anhui 230026, China*

(Dated: November 26, 2021)

We study the history-dependent percolation in two dimensions, which evolves in generations from standard bond-percolation configurations through iteratively removing occupied bonds. Extensive simulations are performed for various generations on periodic square lattices up to side length $L = 4096$. From finite-size scaling, we find that the model undergoes a continuous phase transition, which, for any finite number of generations, falls into the universality of standard 2D percolation. At the limit of infinite generation, we determine the correlation-length exponent $1/\nu = 0.828(5)$ and the fractal dimension $d_f = 1.8644(7)$, which are not equal to $1/\nu = 3/4$ and $d_f = 91/48$ for 2D percolation. Crossover phenomena between the two universalities are clearly observed. The transition in the infinite generation falls outside the standard percolation universality, and apparently differs from the discontinuous transition of history-dependent percolation on random networks.

I. INTRODUCTION

Percolation, originally proposed for modeling transport behavior in a random medium [1], has numerous applications in various areas of science and technologies [2]. In the standard bond percolation on a given lattice, each bond is independently occupied with probability p , and a cluster corresponds to a set of sites connected together by occupied bonds. As p increases, the bond percolation undergoes a continuous transition at percolation threshold p_c from a state of locally connected sites to the percolating phase with an infinitely spanning cluster [3]. In two dimensions, the critical exponents $\nu = 4/3$ (for correlation length) and $\beta/\nu = 5/48$ (for order parameter) are predicted by conformal field theory [4], Coulomb gas theory [5] and stochastic Loewner evolution [6] and confirmed exactly in the triangular-lattice site percolation [7]. In the renormalization-group treatment, these exponents are related to the thermal and magnetic renormalization exponents as $y_t = 1/\nu = 3/4$ and $y_h = 2 - \beta/\nu = 91/48$. The magnetic exponent y_h is also frequently referred to the fractal dimension d_f for critical percolation clusters.

The nature of percolation transitions is a central topic and the conventional percolation transitions are mostly continuous [8]. The search for discontinuous percolation transition stemmed from the exploration of bootstrap percolation [9–11], and renewed in recent studies for the explosive percolation [12–18] and the cascading failure model [19, 20]. Nevertheless, the explosive percolation transitions on random graphs [13, 16, 17] and square lattices [14, 15] were eventually demonstrated to be continuous. Besides, constant attention has been paid to the critical phenomena of percolation models involving manipulations of cluster structures [21–25].

Recently, the history-dependent percolation was introduced to model human brain networks, social networks and the spread of diseases [25]. At the beginning, for a given graph, two standard, uncorrelated bond configurations are generated with probability p , labeled as generation $n = 0$ and 1. An ef-

fective coupling is turned on between the two configurations as follows. An occupied bond at $n = 0$ is deleted iff its two ending sites belong to different clusters in the $n = 1$ configuration. Applying this operation to each occupied bond at $n = 0$ deterministically leads to a new configuration, which is specified by $n = 2$. Analogously, the $n = 3$ configuration is obtained from $n = 1$ according to its coupling to the $n = 2$ configuration. Repeat this procedure until no more bonds can be removed, for which the generation is denoted as \mathcal{I} [26]. An illustration is given in Fig. 1. It is clear that the $n = 0$ and 1 percolation is simply the standard bond percolation, and for $n \geq 2$, it is called the history-dependent percolation. In the $n \rightarrow \infty$ limit, the configurations are taken as those at $n = \mathcal{I}$. In Ref. [25], the model was studied on randomly networked structures including Erdős–Rényi networks and scale-free networks, and it was shown that the transitions at finite generations belong to the mean-field percolation universality class, whereas a discontinuous transition emerges at the infinite generation.

Using extensive Monte Carlo simulations, we investigate the critical behavior of the history-dependent percolation on periodic square lattices. A phase diagram is given in Fig. 2. For finite generations $n = 2, 4$ and 7, we find that the model exhibits a continuous transition having critical exponents $y_t = 3/4$ and $y_h = 91/48$ and belonging to the universality class of two-dimensional (2D) standard percolation. For the infinite generation $n \rightarrow \infty$, we observe a continuous transition at $p_c = 0.576132(2)$ with the critical exponents $y_t = 0.828(5)$ and $y_h = 1.8644(7)$ beyond the standard percolation universality. The continuous transition for $n \rightarrow \infty$ is further confirmed from the critical distribution function $P(\mathcal{C}_1, L)$ of the largest-cluster size \mathcal{C}_1 , which follows a single-variable function $\tilde{P}(x)$ with $P(\mathcal{C}_1, L)d\mathcal{C}_1 = \tilde{P}(x)dx$ [$x \equiv \mathcal{C}_1/L^{d_f}$, $d_f = y_h = 1.8644(7)$]. In addition, at p_c , the cluster-number density $n(s, L)$ of size s obeys the standard scaling formula $n(s, L) \sim s^{-\tau} \tilde{n}(s/L^{d_f})$ of a continuous transition, with the hyper-scaling relation $\tau = 1 + 2/d_f$. Moreover, we find a continuous crossover between the critical behavior at finite and infinite generations.

The remainder of the paper is organized as follows. Section II introduces numerical methodology with an emphasis

* jplv2014@ahnu.edu.cn

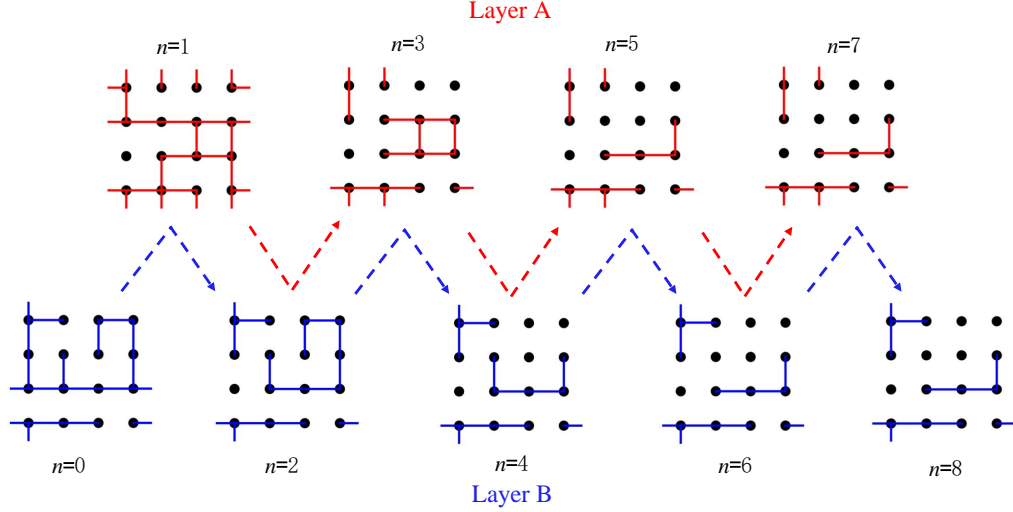


Figure 1. Illustration for the evolution in the history-dependent percolation on a periodic square lattice. Generations $n = 0$ and $n = 1$ are independent configurations produced by a random process as of standard bond percolation. The generation n with $n \geq 2$ evolves from the prior generation $n - 2$ in the same layer, with the input from generation $n - 1$ in the other layer: for each occupied bond in generation $n - 2$, if its two ending sites belong to different clusters in generation $n - 1$, remove the occupied bond. The process is halted once two consecutive evolutions do not make any change to configurations. For this specific example, the generation number after the last evolution is $\mathcal{I} = 8$.

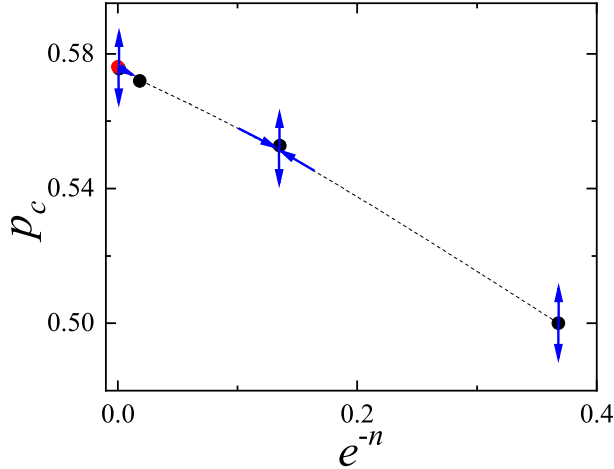


Figure 2. Phase diagram of the history-dependent percolation on the square lattice. At a finite n , the continuous phase transition has critical exponents $y_t = 3/4$ and $y_h = 91/48$. At the infinite generation $n \rightarrow \infty$, there is a continuous transition with critical exponents $y_t = 0.828(5)$ and $y_h = 1.8644(7)$. Here, we plot percolation threshold p_c versus e^{-n} to indicate the fast convergence of $p_c(n)$ to $p_c(n \rightarrow \infty) = 0.576132(2)$ as n increases, in the sense that the p_c versus e^{-n} relation is close to a linear behavior. The renormalization flows around fixed points are sketched.

on sampled quantities. Section III presents numerical results. Specifically speaking, subsections III A and III B present the determination of the percolation thresholds and the critical exponents y_t and y_h , respectively. Subsection III C demonstrates the geometric properties of critical clusters for $n \rightarrow \infty$. Sub-

section III D reveals the crossover behavior of critical phenomena from infinite to finite generations. A discussion is finally given in Sec. IV.

II. MONTE CARLO METHOD AND SAMPLED QUANTITIES

We perform Monte Carlo simulations for the history-dependent percolation on periodic square lattices with side length L ranging from $L = 8$ to 4096. For each generation of percolation configurations, we identify clusters of connected sites using the breadth-first search, and sample various observables such like those in high-precision Monte Carlo studies of standard percolation models [27–29]. More specifically speaking, the following observables are defined:

- The number of occupied bonds \mathcal{N} . In particular, for the initial configurations of layers A and B we label the numbers of occupied bonds as \mathcal{N}_{A_0} and \mathcal{N}_{B_0} respectively, and denote the total number as $\mathcal{N}_0 = \mathcal{N}_{A_0} + \mathcal{N}_{B_0}$.
- The size \mathcal{C}_1 of the largest cluster.
- The second moment of cluster-size distribution $\mathcal{S}_2 = \sum_C |C|^2$, where the summation runs over all clusters.
- The observables $\mathcal{R}^{(x)}$ and $\mathcal{R}^{(y)}$, which equal 1 if a cluster wraps around the periodic lattice in x and y direction, respectively, and equal 0 otherwise.

For each generation, we sample the following quantities using aforementioned observables:

- The mean size of the largest cluster $C_1 = \langle \mathcal{C}_1 \rangle$.
- A susceptibility-like quantity $\chi = \langle \mathcal{S}_2 \rangle / L^2$.
- The wrapping probability

$$R^{(h)} = \langle \mathcal{R}^{(x)} \rangle = \langle \mathcal{R}^{(y)} \rangle, \quad (1)$$

which gives the probability that a wrapping exists in the x direction. In particular, for the 2D *standard* percolation, the critical value $R_c^{(h)} = 0.521\,058\,290$ is exact in the $L \rightarrow \infty$ limit [30].

- The covariance of $\mathcal{R}^{(x)}$ and \mathcal{N}_0 as

$$g_{bR}^{(h)} = \langle \mathcal{R}^{(x)} \mathcal{N}_0 \rangle - \langle \mathcal{R}^{(x)} \rangle \langle \mathcal{N}_0 \rangle, \quad (2)$$

which relates to the derivative of $R^{(h)}$ with respect to p as $g_{bR}^{(h)} = p(1-p) \frac{dR^{(h)}}{dp}$.

The generation number \mathcal{I} of the ending configuration is an indicator for the length of effective evolution. Accordingly, the quantity n_{\max} is defined as

$$n_{\max} = \langle \mathcal{I} \rangle. \quad (3)$$

For analyzing continuous phase transitions, we employ the tool of finite-size scaling (FSS) theory, which predicts that a quantity Q near criticality scales as

$$Q(L, p) = L^{X_Q} \tilde{Q}((p - p_c)L^{y_t}), \quad (4)$$

where \tilde{Q} is a scaling function. The scaling exponent X_Q is quantity-dependent. For the quantities such like $R^{(h)}$, C_1 , χ and $g_{bR}^{(h)}$, the scaling exponents are given as $X_Q = 0$, y_h , $2y_h - 2$ and y_t , respectively.

III. NUMERICAL RESULTS

A. Percolation thresholds

Firstly, we address the situations with finite n . The finite-size Monte Carlo data of the wrapping probability $R^{(h)}$ are plotted in Figs. 3(a), (b) and (c) for $n = 2, 4$ and 7 , respectively. For each n , the intersections of the $R^{(h)}$ versus p curves for $L \rightarrow \infty$ are around a finite bond-occupation probability p_c . Meanwhile, the vertical coordinates for the intersections converge to a finite value around 0.521 , which seems universal among these finite generations and agrees with the exact value $R_c^{(h)} = 0.521\,058\,290$ of continuous transition in 2D standard percolation.

More precisely, we fit the Monte Carlo data of $R^{(h)}$ to the formula

$$R^{(h)}(L, p) = R_c^{(h)} + a_1(p - p_c)L^{y_t} + a_2(p - p_c)^2 L^{2y_t} + \dots + b_1 L^{-\omega_1} + b_2 L^{-2} + \dots \quad (5)$$

which is an explicit form of (4) for $Q = R^{(h)}$ with additional finite-size correction terms b_1 and b_2 . The critical wrapping

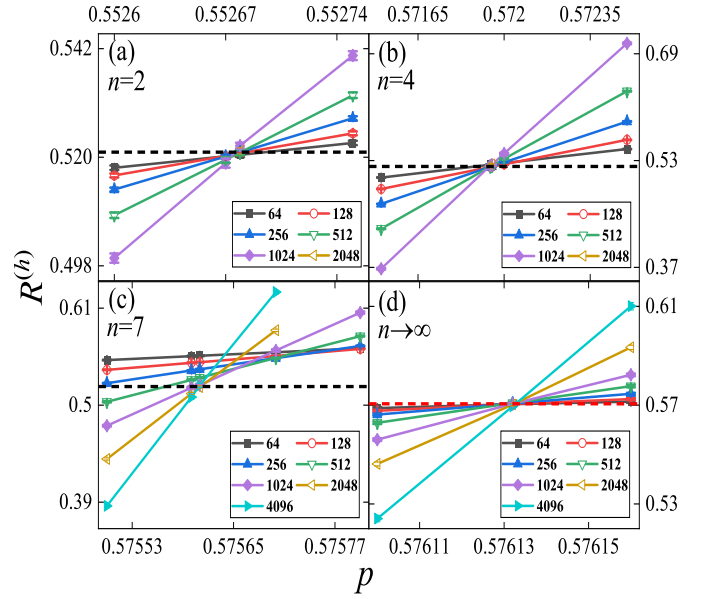


Figure 3. Wrapping probability $R^{(h)}$ versus p for the finite generations $n = 2$ (a), 4 (b) and 7 (c) and for the infinite generation $n \rightarrow \infty$ (d) with various sizes. The black dashed lines in panels (a), (b) and (c) represent the exact value $R_c^{(h)} = 0.521\,058\,290$ of standard percolation universality, while the red dashed line in panel (d) denotes the estimate $R_c^{(h)} = 0.570\,5$ for $n \rightarrow \infty$.

probability $R_c^{(h)}$ is expected to be universal among the transitions in the same universality and on the same lattice geometry. The parameters a_k and b_l ($k = 1, 2, \dots; l = 1, 2, \dots$) are non-universal. The leading correction exponent is denoted as ω_1 , while the subleading correction term is fixed to be L^{-2} . Fits are performed using the least-squares method. In these fits and for those mentioned elsewhere in the manuscript, we try to include subleading terms, such like the a_2 , b_1 and b_2 terms in Eq. (5), or their combinations. This would be useful for a systematical justification on the evidence level of fits. Besides, preferred fits should feature a stability against varying L_{\min} that denotes the minimum size incorporated, and ensure that the Chi squared χ^2 per degree of freedom (DF) is not larger than $\mathcal{O}(1)$.

For the finite generation $n = 2$, we firstly include the correction terms with b_1 and b_2 , and obtain $p_c = 0.552\,679(6)$, $y_t = 0.74(4)$ and $R_c^{(h)} = 0.522(7)$. These estimates for y_t and $R_c^{(h)}$ further imply a transition in the standard percolation universality. As $R_c^{(h)}$ is fixed to be $R_c^{(h)} = 0.521\,058\,290$, we have $p_c = 0.552\,678(1)$, $y_t = 0.75(4)$ and $\omega_1 = 1.2(4)$. As $y_t = 3/4$ and $\omega_1 = 1$ are both fixed, we obtain $p_c = 0.552\,678(2)$ and $R_c^{(h)} = 0.521\,1(4)$. On this basis, we let $y_t = 3/4$, $R_c^{(h)} = 0.521\,058\,290$ and $\omega_1 = 1$ all fixed for reducing uncertainties, and obtain $p_c = 0.552\,677\,6(9)$.

Similar analyses are performed for $n = 4$, for which the results of fits can be found in Table I.

As indicated by Fig. 3(c), the finite-size corrections become severe for $n = 7$. Hence, simulation results for large lattices

Table I. Fits of $R_c^{(h)}$ to (5) for the finite generations $n = 2, 4$ and 7 and for the infinite generation $n \rightarrow \infty$.

n	p_c	$R_c^{(h)}$	y_t	ω_1	$\chi^2/\text{DF}/L_{\min}$
2	0.552 679(6)	0.522(7)	0.74(4)	0(2)	3.7/15/16
	0.552 678(1)	0.521 058 29	0.75(4)	1.2(4)	3.8/19/8
	0.552 678(2)	0.521 1(4)	3/4	1	3.7/17/16
	0.552 677 6(9)	0.521 058 29	3/4	1	3.7/18/16
4	0.571 940(3)	0.520(2)	0.743(6)	2(4)	7.4/15/64
	0.571 941(1)	0.521 058 29	3/4	1.0(5)	8.8/17/64
	0.571 941(2)	0.521 0(8)	3/4	1	8.8/17/64
	0.571 941(1)	0.521 058 29	3/4	1	8.6/14/128
7	0.575 613(1)	0.521 058 29	0.77(1)	1.2(1)	12.3/12/128
	0.575 607(4)	0.518(3)	0.72(5)	-	0.3/2/2048
	0.575 608(3)	0.519(3)	3/4	-	0.7/3/2048
∞	0.576 132 3(5)	0.570 7(2)	0.85(2)	-	8.1/11/256
	0.576 132 2(6)	0.570 7(3)	0.85(2)	-	7.9/8/512
	0.576 131 7(8)	0.570 2(6)	0.86(3)	-	6.7/5/1024

are a must to achieve an extensive set of preferred fits. As we fix $R_c^{(h)} = 0.521\,058\,290$, we find $p_c = 0.575\,613(1)$, $y_t = 0.77(1)$ and $\omega_1 = 1.2(1)$. As we incorporate merely large enough sizes with $L_{\min} = 2048$ and preclude correction terms, the results are $p_c = 0.575\,607(4)$, $y_t = 0.72(5)$ and $R_c^{(h)} = 0.518(3)$. As $y_t = 3/4$ is further fixed, we obtain $p_c = 0.575\,608(3)$ and $R_c^{(h)} = 0.519(3)$.

For the infinite generation $n \rightarrow \infty$, the $R^{(h)}$ versus p curves are plotted in Fig. 3(d), which demonstrates that the intersections are located around $p_c \approx 0.576\,13$, where $R^{(h)}$ is close to $R_c^{(h)} \approx 0.570$. The intersections are nearly coincident at $(0.576\,13, 0.570)$, indicating a continuous transition. The coincidence further indicates minor corrections in the FSS. Hence, in the fits according to (5), we drop the correction terms and examine the stability of fits by varying L_{\min} . As shown in Table I, we find consistent results over the fits with $L_{\min} = 256, 512$ and 1024 . Our final estimates of p_c and $R_c^{(h)}$ are $p_c = 0.576\,132(2)$ and $R_c^{(h)} = 0.570\,5(8)$, respectively.

In summary, by comparing preferred fits, we estimate percolation thresholds as precise as $p_c = 0.552\,678(2)$ ($n = 2$), $0.571\,941(4)$ ($n = 4$), $0.575\,61(1)$ ($n = 7$) and $0.576\,132(2)$ ($n \rightarrow \infty$), where the error bars consist of one statistical error and a subjective estimate of systematic error. For the finite generations, the estimates $R_c^{(h)} = 0.521\,2(6)$ ($n = 2$), $0.521(2)$ ($n = 4$) and $0.519(4)$ ($n = 7$) of critical wrapping probability agree well with the exact value $R_c^{(h)} = 0.521\,058\,290$ of 2D standard percolation. Moreover, we find that the correction term $L^{-\omega_1}$ ($\omega_1 \approx 1.2$) emerges, which is distinct from the leading correction term L^{-2} of the critical wrapping probabilities in standard percolation [30]. We note that the correction exponent $\omega_1 = 3/2$ was also found for 2D percolation [31]. On the other hand, the estimate $R_c^{(h)} = 0.570\,5(8)$ for $n \rightarrow \infty$ indicates a new universality.

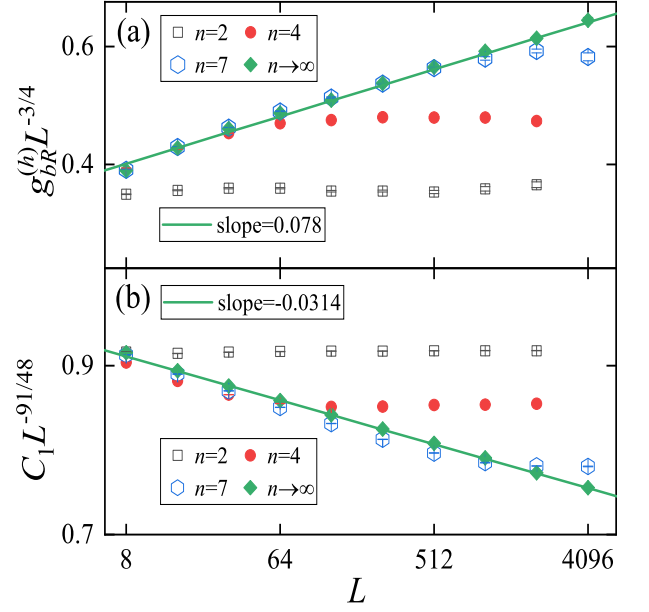


Figure 4. Illustration for the estimated critical exponents y_t and y_h by scaled quantities $g_{bR}^{(h)} L^{-3/4}$ (a) and $C_1 L^{-91/48}$ (b). For the finite generations $n = 2, 4$ and 7 , the scaled data are asymptotically constants as L increases, confirming the estimates of the critical exponents as $y_t = 3/4$ and $y_h = 91/48$. For the infinite generation $n \rightarrow \infty$, deviations from the behavior of standard percolation universality are indicated by the linearities of scaled data with non-zero slopes. These slopes take values 0.078 and -0.0314 , which measure the deviations from $y_t = 0.828(5)$ and $y_h = 1.864\,4(7)$ of the infinite generation to $y_t = 3/4$ and $y_h = 91/48$ of the standard universality, respectively.

B. Critical exponents y_t and y_h

We now focus on the Monte Carlo data at the above-estimated percolation threshold p_c , where the FSS formula (4) is simplified as

$$Q(L, p_c) = L^{X_Q} (a_0 + b_1 L^{-1} + b_2 L^{-2} + \dots) \quad (6)$$

with finite-size correction terms b_1 and b_2 being incorporated, and a_0 representing a constant. In some cases, a constant term c_0 from analytic background should be included in addition to (6).

We estimate the critical exponent y_t from the covariance $g_{bR}^{(h)}$ which relates to the derivative $dR^{(h)}/dp$. Fits are performed according to (6) with $X_Q = y_t$. For $n = 2$, we obtain $y_t = 0.751(3)$ with $\chi^2/\text{DF}=1.3/2$ and $L_{\min} = 128$, as the constant term c_0 and the correction terms b_1 and b_2 are not included. Similarly, for $n = 4$, we obtain $y_t = 0.747(3)$ with $\chi^2/\text{DF}=1.1/2$ and $L_{\min} = 256$. For $n = 7$, stable fits are achieved if c_0 term is present. Accordingly, we have $y_t = 0.76(1)$ with $\chi^2/\text{DF}=0.1/1$ and $L_{\min} = 256$. The final estimate of y_t for each of the finite generations is achieved by comparing preferred fits. As summarized in Table II, the results of y_t consist with the exact value $y_t = 3/4$ of standard 2D percolation. For the infinite generation $n \rightarrow \infty$, as listed

Table II. Percolation thresholds p_c , critical exponents y_t and y_h , and critical wrapping probabilities $R_c^{(h)}$ for the finite generations $n=2, 4$ and 7 . Exact values in the 2D standard universality class are listed as well for comparison.

n	2	4	7	exact
p_c	0.552 678(2)	0.571 941(4)	0.575 61(1)	-
y_t	0.751(5)	0.74(1)	0.75(2)	3/4
y_h	1.896 0(3)	1.896 5(8)	1.895(2)	91/48
$R_c^{(h)}$	0.521 2(6)	0.521(2)	0.519(4)	0.521 058 290

in Table III, we obtain $y_t = 0.827(1)$, $0.829(1)$ and $0.827(2)$, with $L_{\min} = 64, 128$ and 256 , respectively. Our final estimate of y_t for $n \rightarrow \infty$ is $y_t = 0.828(5)$; the error bar is enlarged, since some finite-size corrections might be ignored in the fitting formula.

For illustrating y_t , we plot in Fig. 4(a) the scaled covariance $g_{bR}^{(h)} L^{-7/4}$ for various generations. For the finite generations $n = 2, 4$ and 7 , the scaled data eventually become constants as L increases. For the infinite generation $n \rightarrow \infty$, deviation from the behavior of standard percolation is demonstrated by the non-zero slope 0.078 , which measures the distance from $y_t = 0.828(5)$ to $y_t = 3/4$.

Another verification for the estimated y_t is provided by Fig. 5, where we plot $R^{(h)}$ versus $(p - p_c)L^{y_t}$ for various n . These plots serve as simultaneous illustrations for the estimated y_t ($3/4$ for $n = 2, 4, 7$ and 0.828 for $n \rightarrow \infty$), the estimated p_c , and the scaling formula (4). For each n , the scaled data of various L collapse compactly on top of each other as $L \rightarrow \infty$.

The critical exponent y_h can be estimated from C_1 and χ according to (6) with $X_Q = y_h$ and $2y_h - 2$, respectively. For $n = 2$, we obtain $y_h = 1.895 9(2)$ by C_1 , and $2y_h - 2 = 1.792 1(4)$ by χ . For $n = 4$, we have $y_h = 1.896 2(5)$ by C_1 , and $2y_h - 2 = 1.792(1)$ by χ . For $n = 7$, we obtain $y_h = 1.894 8(9)$ by C_1 , and $2y_h - 2 = 1.792(2)$ by χ . The final estimates of y_h for the finite generations are given as $1.896 0(3)$ ($n = 2$), $1.896 5(8)$ ($n = 4$) and $1.895(2)$ ($n = 7$), which are consistent with the exact value $y_h = 91/48$ of the standard percolation. The results for the infinite generation $n \rightarrow \infty$ are exemplified in Table III, for which our final estimate of y_h is $y_h = 1.864 4(7)$.

In Fig. 4(b), the scaled data $C_1 L^{-91/48}$ for the finite generations converge to constants as L increases, confirming $y_h = 91/48$. Meanwhile, the scaled data for $n \rightarrow \infty$ clearly deviate from the behavior in standard universality and confirm $y_h = 1.864 4(7)$.

Moreover, as demonstrated by Fig. 4, the quantities $g_{bR}^{(h)}$ and C_1 exhibit more severe finite-size corrections as the finite n increases.

C. Geometric properties of critical clusters

We have found that the transition for the infinite generation $n \rightarrow \infty$ is continuous and falls outside the universality of the

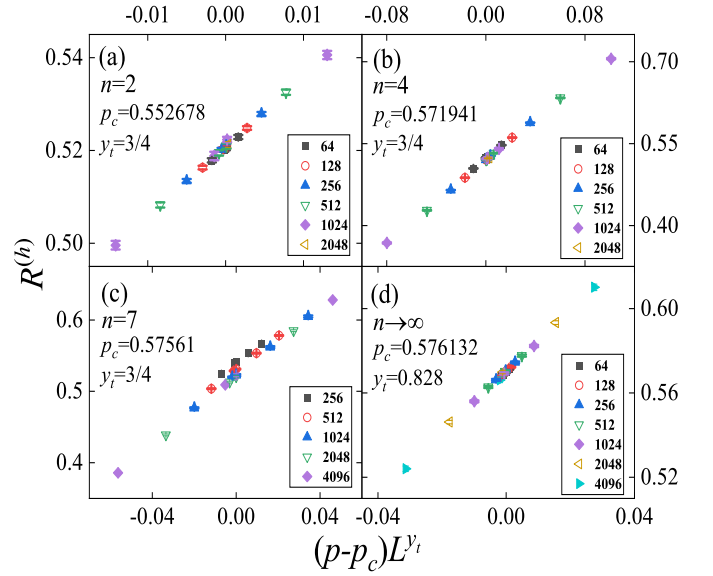


Figure 5. Illustration for the scaling formula (4) with $Q = R^{(h)}$. In panels (a), (b) and (c), the $R^{(h)}$ data for the finite generations are plotted against $(p - p_c)L^{y_t}$ with $y_t = 3/4$ and $p_c = 0.552 678$ ($n = 2$), $0.571 941$ ($n = 4$) and $0.575 61$ ($n = 7$). In panel (d), the $R^{(h)}$ data for the infinite generation $n \rightarrow \infty$ are plotted with $y_t = 0.828$ and $p_c = 0.576 132$.

Table III. Fits of $g_{bR}^{(h)}$, C_1 and χ to (6) for the infinite generation $n \rightarrow \infty$. The scaling exponents X_Q for $g_{bR}^{(h)}$, C_1 and χ are y_t , y_h and $2y_h - 2$, respectively. Our final estimates $y_t = 0.828(5)$ and $y_h = 1.864 4(7)$ are based on comparing all preferred fits of these quantities.

Q	X_Q	$\chi^2/\text{DF}/L_{\min}$
$g_{bR}^{(h)}$	0.827(1)	11.0/5/64
	0.829(1)	3.9/4/128
	0.827(2)	2.5/3/256
C_1	1.864 7(1)	14.2/5/32
	1.864 3(2)	4.6/4/64
	1.864 0(3)	2.1/3/128
χ	1.729 1(1)	7.4/5/64
	1.729 3(1)	5.4/4/128
	1.729 1(2)	4.5/3/256

standard percolation. In following, we further explore the geometric properties of critical clusters. We investigate the critical probability distribution of the largest-cluster size as well as the critical cluster-number density, and examine their compatibility with the FSS theory of continuous geometric transition.

The critical distribution function $P(C_1, L)$ for the largest-cluster size C_1 is shown in Fig. 6(a). At the critical bond-occupation probability $p_c = 0.576 132$ (shown in the plot) and away from p_c , we do not find a stable double-peaked structure, confirming the absence of discontinuous transition. Further, as displayed in Fig. 6(b), the distribution $P(C_1, L)dC_1$ can be rescaled into a single-variable form as $\tilde{P}(x)dx$ with

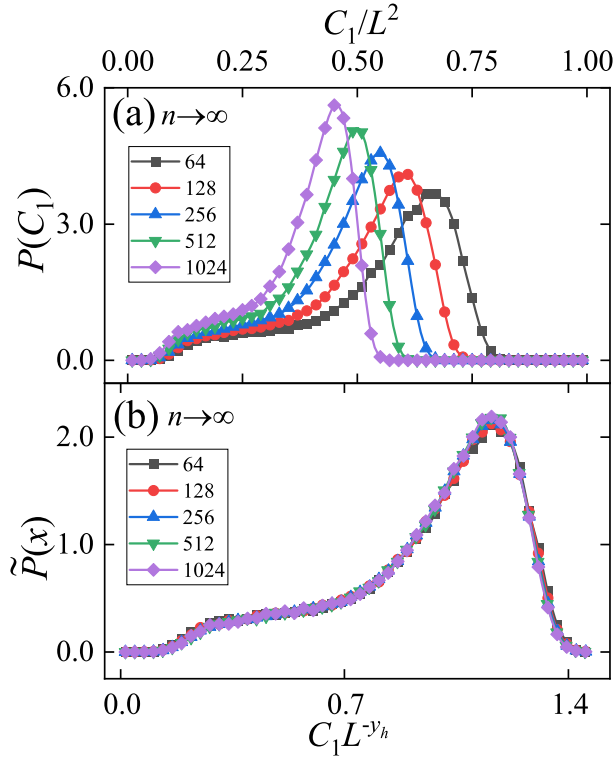


Figure 6. Critical distribution function $P(C_1, L)$ for the scaled size $C_1 L^{-2}$ of the largest cluster in the infinite generation $n \rightarrow \infty$. The data are for $p_c = 0.576132$. In panel (b), the rescaled critical distribution function $\tilde{P}(x)$ ($x \equiv C_1/L^{y_h}$) shows a single-variable behavior.

$x \equiv C_1/L^{d_f}$ and $d_f = y_h$. The absence of double-peaked structure and the single-variable behavior in the distribution function are indicators for a continuous geometric transition.

We also analyze the cluster-number density $n(s, L)$ of cluster size s . At a continuous phase transition, it is expected that

$$n(s, L) = s^{-\tau} \tilde{n}(s/L^{d_f}), \quad (7)$$

where \tilde{n} is a scaling function and $\tau = 1 + 2/d_f$. As shown in Fig. 7(a), the large- s asymptotics of $n(s, L)$ is consistent with the power law $s^{-\tau}$, where the exponent $\tau = 2.0727$ is given by $d_f = y_h = 1.8644$. Figure 7(b) plots $s^\tau n(s, L)$ versus s/L^{d_f} for various L and demonstrates a compact collapse. The FSS formula (7) is hence confirmed for the percolation transition in the infinite generation $n \rightarrow \infty$.

D. Continuous crossover

A continuous crossover of critical behavior from infinite to finite generation has been indicated by Fig. 4, as the $n = 7$ and $n \rightarrow \infty$ data are close at small sizes but deviate at larger sizes. In following, we further illustrate the crossover phenomena.

Figure 8 displays a collapse of the critical wrapping probabilities $R^{(h)}(L, p_c)$ versus an n -dependent rescaled size L_r . We define $L_r = L/r(n)$ with the rescaled factor $r(n)$ chosen

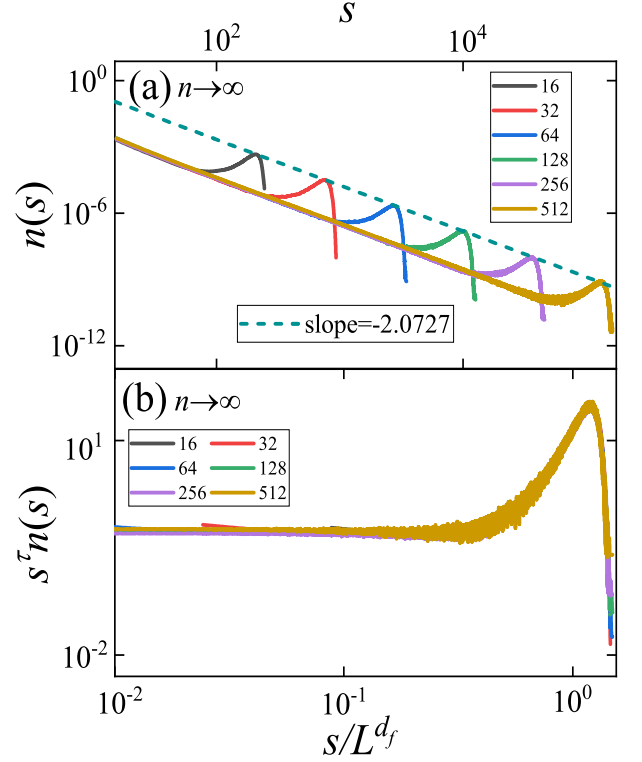


Figure 7. Cluster-number density $n(s, L)$ of various L at the percolation threshold $p_c = 0.576132$ in the infinite generation $n \rightarrow \infty$. In panel (a), the dashed line has a slope of $-\tau$ with $\tau = 1 + 2/d_f \approx 2.0727$. A scaling analysis according to (7) is shown in panel (b).

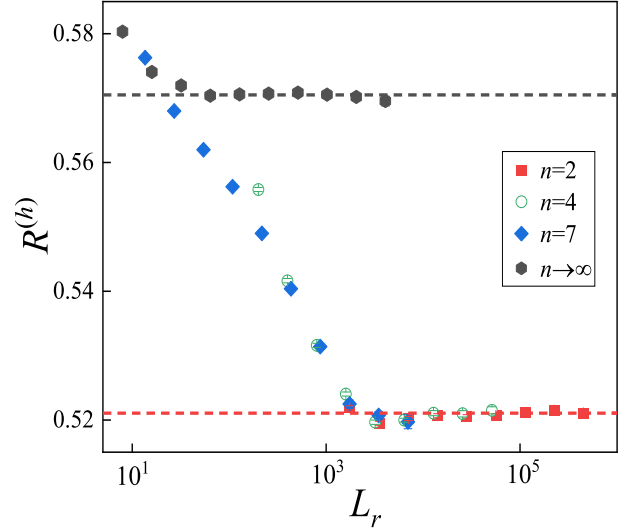


Figure 8. Finite-size $R^{(h)}$ data at p_c versus rescaled size $L_r = L/r(n)$ for finite and infinite generations. The rescaled factor $r(n)$ is generation-dependent. The asymptotic values (represented by dashed lines) in the $L_r \rightarrow \infty$ limit are $0.5705(8)$ and 0.521058290 .

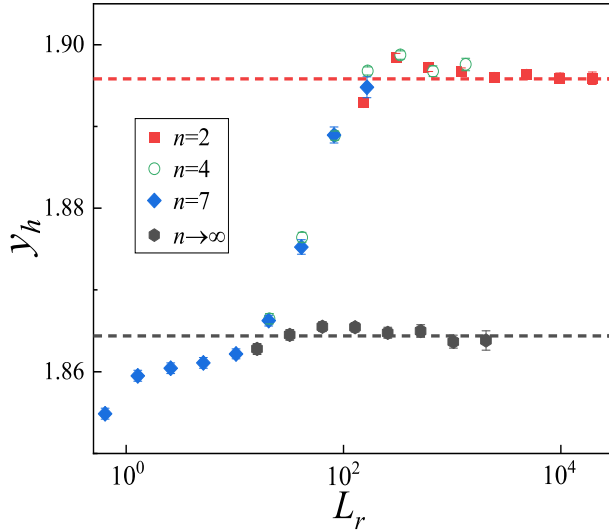


Figure 9. Finite-size estimates of the effective magnetic exponent y_h , determined from C_1 at p_c , versus rescaled size L_r . The asymptotic values (represented by dashed lines) in the $L_r \rightarrow \infty$ limit are 1.8644(7) and 91/48.

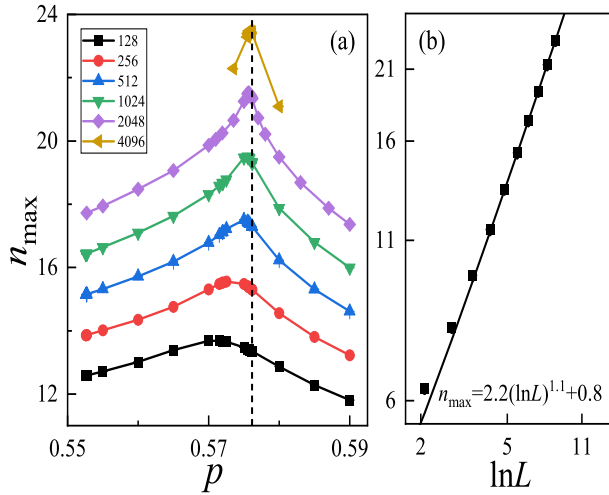


Figure 10. Quantity n_{\max} versus p for various L (a) and versus $\ln L$ at $p = 0.576132$ in a log-log scale (b). The dashed line in panel (a) marks the position $p = 0.576132$ and the solid line in panel (b) represents the logarithmic divergence $n_{\max} = 2.2(\ln L)^{1.1} + 0.8$.

such that the $R^{(h)}$ versus L_r data of various n collapse on top of each other. As a result, the small-size data for $n = 7$ are close to the data for $n \rightarrow \infty$. As L_r increases, however, the $n = 7$ data tend to collapse with those for $n = 2$ and 4.

The crossover can also be seen in the size-dependent effective magnetic exponent $y_h(L)$, which is determined from C_1 with sizes L and $2L$ by the formula $y_h(L) = \ln[C_1(2L, p_c)/C_1(L, p_c)]/\ln 2$. The results are given in Fig. 9, which demonstrates a crossover between the asymptotic behavior of $n = 7$ data. At small sizes the $n = 7$ data are in the same profile with $n \rightarrow \infty$, whereas at large sizes they collapse

with the data of $n = 2$ and 4. Moreover, we see the crossover behavior from the effective thermal exponent $y_t(L)$ extracted by $g_{bR}^{(h)}$ (not shown), albeit it suffers from huge statistical errors.

IV. DISCUSSION

By using extensive Monte Carlo simulations, we study the critical behavior for the history-dependent percolation on the square lattice. At finite generations $n = 2, 4$ and 7, we locate percolation transitions at $p_c = 0.552678(2)$, $0.571941(4)$ and $0.57561(1)$ respectively. We find that these transitions belong to the universality class of standard percolation in two dimensions, although finite-size corrections become larger when n increases, as demonstrated in Figs. 3, 4 and 5. At the infinite generation $n \rightarrow \infty$, we observe a continuous transition at $p_c = 0.576132(2)$ with the critical exponents $y_t = 0.828(5)$ and $y_h = 1.8644(7)$ and the critical wrapping probability $R_c^{(h)} = 0.5705(8)$, which fall outside the standard percolation universality. The critical distribution function $P(C_1, L)$ and the critical cluster-number density $n(s, L)$ follow the standard scaling behavior of a continuous geometric transition. Furthermore, we obtain complementary evidence confirming a continuous crossover of critical behavior from the infinite to the finite generations. This evidence comes from $g_{bR}^{(h)}$, C_1 and $R^{(h)}$ and from effective critical exponents.

The evolution process of history-dependent percolation needs a deeper understanding. To this end, we analyze the quantity n_{\max} . As displayed in Fig. 10(a), the n_{\max} data reaches a maximum around $p = 0.576132$. This feature becomes obvious as $L \rightarrow \infty$. As we have known, the bond-occupation probability $p = 0.576132$ is the percolation threshold of the infinite generation. Hence, at $p_c = 0.576132$, initial percolation configurations typically have the largest number of iterative bond deletions before reaching the infinite-generation configurations, which are critical. As shown in Fig. 10(b), the critical n_{\max} data diverge logarithmically as $L \rightarrow \infty$. Specifically speaking, the data can be fitted to the formula $n_{\max} = g(\ln L)^{\hat{x}} + n_{\max}^0$, with $g \approx 2.2$, $\hat{x} \approx 1.1$ and $n_{\max}^0 \approx 0.8$.

There are a number of open questions to be explored, as motivated by this work. For example, what are the exact values of the critical exponents $y_t = 0.828(5)$ and $y_h = 1.8644(7)$ for the infinite generation? Can they be obtained within the framework of conformal field theories or Coulomb gas theory? In addition, it is noted that the history-dependent percolation can be extended such that it has an arbitrary number N_ℓ of layers. In the present $N_\ell = 2$ model shown in Fig. 1, the inter-layer coupling looks like A-B-A'-B'-..., and thus has an effective period of 2. For $N_\ell \geq 3$, the configuration coupling looks like A-B-C...-A'-B'-C'..., and the coupling period is longer. This indicates that the overlap between two subsequent configurations on the same layer, A and A', becomes smaller. In the infinite-generation limit, percolation clusters are either very dense or very small to resist the bond-deletion action. A first-order percolation transition may arise for some

large N_ℓ and finite generation n . An intriguing scenario then can happen: for a given large N_ℓ , there exists a “tricritical” value of n , separating a line of continuous and first-order percolation transitions. Finally, it would be also interesting to explore the history-dependent percolation in higher spatial dimension $d \geq 3$. We leave these questions for further studies.

ACKNOWLEDGMENTS

Acknowledgements. YD is indebted to Ming Li and Linyuan Lü for valuable discussions. This work has been supported by the National Natural Science Foundation of China under Grant Nos. 11774002, 11625522 and 11975024.

-
- [1] S. R. Broadbent and J. M. Hammersley, *Percolation processes: I. Crystals and mazes*, in *Mathematical Proceedings of the Cambridge Philosophical Society*, Vol. 53 (1987) pp. 629–641.
 - [2] G. Grimmett, *Percolation* (Springer, 1999).
 - [3] D. Stauffer and A. Aharony, *Introduction to percolation theory* (CRC press, 2018).
 - [4] J. L. Cardy, *Conformal invariance*, in *Phase Transitions and Critical Phenomena*, Eds. C. Domb, M. Green and J. L. Lebowitz (Academic Press, London, 1987).
 - [5] B. Nienhuis, *Two-dimensional critical phenomena and the Coulomb Gas*, in *Phase Transitions and Critical Phenomena*, Eds. C. Domb, M. Green and J. L. Lebowitz (Academic Press, London, 1987).
 - [6] G. F. Lawler, O. Schramm, and W. Werner, “The dimension of the planar brownian frontier is $4/3$,” *Math. Res. Lett.* **8**, 401–411 (2000).
 - [7] S. Smirnov and W. Werner, “Critical exponents for two-dimensional percolation,” *Math. Res. Lett.* **8**, 729–744 (2001).
 - [8] N. Araújo, P. Grassberger, B. Kahng, K. J. Schrenk, and R. M. Ziff, “Recent advances and open challenges in percolation,” *Eur. Phys. J. Spec. Top.* **223**, 2307–2321 (2014).
 - [9] J. Chalupa, P. L. Leath, and G. R. Reich, “Bootstrap percolation on a bethe lattice,” *J. Phys. C: Solid State Physics* **12**, L31 (1979).
 - [10] J. Adler, “Bootstrap percolation,” *Physica A* **171**, 453–470 (1991).
 - [11] J.-O. Choi and U. Yu, “Bootstrap and diffusion percolation transitions in three-dimensional lattices,” *arXiv preprint* **2020**, [arXiv:2004.11487](https://arxiv.org/abs/2004.11487).
 - [12] D. Achlioptas, R. M. D’Souza, and J. Spencer, “Explosive percolation in random networks,” *Science* **323**, 1453–1455 (2009).
 - [13] E. J. Friedman and A. S. Landsberg, “Construction and analysis of random networks with explosive percolation,” *Phys. Rev. Lett.* **103**, 255701 (2009).
 - [14] F. Radicchi and S. Fortunato, “Explosive percolation: A numerical analysis,” *Phys. Rev. E* **81**, 036110 (2010).
 - [15] R. M. Ziff, “Scaling behavior of explosive percolation on the square lattice,” *Phys. Rev. E* **82**, 051105 (2010).
 - [16] R. A. da Costa, S. N. Dorogovtsev, A. V. Goltsev, and J. F. F. Mendes, “Explosive percolation transition is actually continuous,” *Phys. Rev. Lett.* **105**, 255701 (2010).
 - [17] O. Riordan and L. Warnke, “Explosive percolation is continuous,” *Science* **333**, 322–324 (2011).
 - [18] H. K. Lee, B. J. Kim, and H. Park, “Continuity of the explosive percolation transition,” *Phys. Rev. E* **84**, 020101 (2011).
 - [19] S. V. Buldyrev, R. Parshani, G. Paul, H. E. Stanley, and S. Havlin, “Catastrophic cascade of failures in interdependent networks,” *Nature* **464**, 1025–1028 (2010).
 - [20] C. Christensen P. Grassberger M. Paczuski S.-W. Son, G. Bizhani, “Percolation theory on interdependent networks based on epidemic spreading,” *EPL (Europhysics Letters)* **97**, 16006 (2012).
 - [21] K. J. Schrenk, M. R. Hilário, V. Sidoravicius, N. A. M. Araújo, H. J. Herrmann, M. Thielmann, and A. Teixeira, “Critical fragmentation properties of random drilling: How many holes need to be drilled to collapse a wooden cube?” *Phys. Rev. Lett.* **116**, 055701 (2016).
 - [22] M. R. Hilário and V. Sidoravicius, “Bernoulli line percolation,” *Stoch. Proc. Appl.* **129**, 5037–5072 (2019).
 - [23] B. Jovanovic, S. V. Buldyrev, S. Havlin, and S. H. Eugene, “Punctuated equilibrium and “history-dependent” percolation,” *Phys. Rev. E* **50**, R2403–R2406 (1994).
 - [24] X.-W. Liu, Y. Deng, and J. L. Jacobsen, “Recursive percolation,” *Phys. Rev. E* **92**, 010103 (2015).
 - [25] M. Li, L. Lü, Y. Deng, M.-B. Hu, H. Wang, M. Medo, and H. E. Stanley, “History-dependent percolation on multiplex networks,” *National Science Review* (2020), [10.1093/nsr/nwaa029](https://doi.org/10.1093/nsr/nwaa029).
 - [26] In actual simulations, we halt the iterations once two consecutive evolutions do not make any change to configurations, and the generation number of ending configuration is taken as \mathcal{I} .
 - [27] R. M. Ziff and M. E. J. Newman, “Convergence of threshold estimates for two-dimensional percolation,” *Phys. Rev. E* **66**, 016129 (2002).
 - [28] J. Wang, Z. Zhou, W. Zhang, T. M. Garoni, and Y. Deng, “Bond and site percolation in three dimensions,” *Phys. Rev. E* **87**, 052107 (2013).
 - [29] X. Xu, J. Wang, J.-P. Lv, and Y. Deng, “Simultaneous analysis of three-dimensional percolation models,” *Front. Phys.* **9**, 113–119 (2014).
 - [30] M. E. J. Newman and R. M. Ziff, “Fast monte carlo algorithm for site or bond percolation,” *Phys. Rev. E* **64**, 016706 (2001).
 - [31] R. M. Ziff, “Correction-to-scaling exponent for two-dimensional percolation,” *Phys. Rev. E* **83**, 020107 (2011).